Mononuclear phagocyte system blockade for enhanced liposome-assisted metabolic glycan labeling and circulating biomarker detection in mice

Pingping Feng[1,2], Tingbi Zhao[1,2], Rundong He[1,2], Lin Gan[1,2], Guangyu Hu[1,2], Xing Chen[1,2,3,4,5,6](✉), Peng Dai[1,2,3,4](✉)

[1] College of Chemistry and Molecular Engineering, Peking University, Beijing 100871, China

[2] Beijing National Laboratory for Molecular Sciences, Peking University, Beijing 100871, China

[3] Synthetic and Functional Biomolecules Center, Peking University, Beijing 100871, China

[4] Key Laboratory of Bioorganic Chemistry and Molecular Engineering of Ministry of Education, Peking University, Beijing 100871, China

[5] Peking-Tsinghua Center for Life Sciences, Peking University, Beijing 100871, China

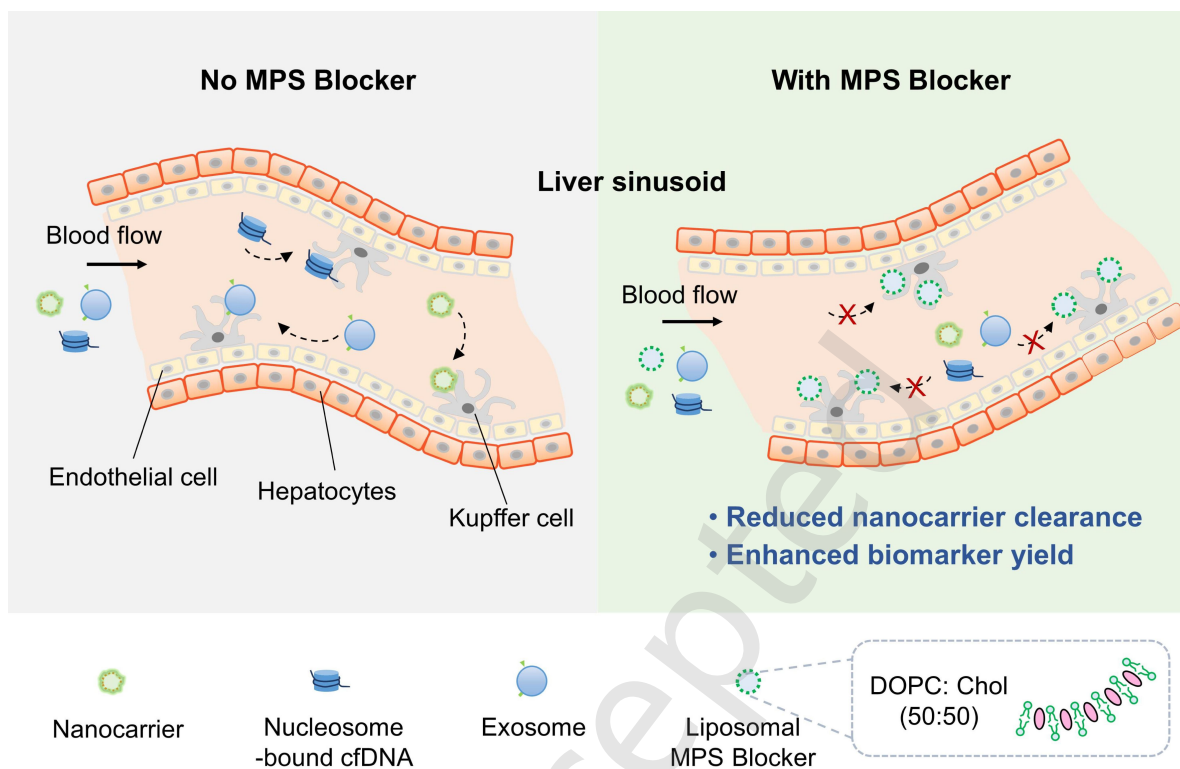[6] College of Chemistry, Beijing Normal University, Beijing 100875, China

Just Accepted

A liposomal mononuclear phagocyte Blocker was developed for enhanced liposome-assisted metabolic glycan labeling and circulating biomarker detection in mice.

Research Article

Mononuclear phagocyte system blockade for enhanced liposome-assisted metabolic glycan labeling and circulating biomarker detection in mice

Pingping Feng[1,2], Tingbi Zhao[1,2], Rundong He[1,2], Lin Gan[1,2], Guangyu Hu[1,2], Xing Chen[1,2,3,4,5,6]✉, and Peng Dai[1,2,3,4]✉

[1]College of Chemistry and Molecular Engineering, Peking University, Beijing 100871, China
[2]Beijing National Laboratory for Molecular Sciences, Peking University, Beijing 100871, China
[3]Synthetic and Functional Biomolecules Center, Peking University, Beijing 100871, China
[4]Key Laboratory of Bioorganic Chemistry and Molecular Engineering of Ministry of Education, Peking University, Beijing 100871, China
[5]Peking-Tsinghua Center for Life Sciences, Peking University, Beijing 100871, China
[6]College of Chemistry, Beijing Normal University, Beijing 100875, China

✉ Address correspondence to Xing Chen, xingchen@pku.edu.cn; Peng Dai, pengdai@pku.edu.cn

ABSTRACT: The rapid clearance of nanoparticles by the mononuclear phagocyte system (MPS) severely compromises nanocarrier delivery efficiency and reduces the isolation yield of circulating biomarkers such as nucleosome-bound cell-free DNA (cfDNA) and exosomes. While liposome-based preconditioning is a promising strategy for transient MPS blockade, effective formulations remain scarce. Here, we report a potent MPS-blocking liposome (the Blocker) identified through an integrated screening strategy combining in vitro Kupffer cell uptake assays with in vivo biodistribution profiling. Notably, even upon co-administration, the Blocker effectively extended the circulation half-life of a widely used FDA‑approved PEGylated liposomal carrier by 2.1 folds, based on which liposome-assisted metabolic glycan labeling was significantly enhanced in a mouse tumor model. Furthermore, liposomal MPS blockade markedly inhibited the clearance of endogenous circulating cfDNA and exosomes, leading to a 6.8-fold increase in recovered cfDNA yield. This work highlighted liposomal blockade as a versatile platform for improving nanoparticle delivery and liquid biopsy sensitivity.

KEYWORDS: mononuclear phagocyte system (MPS) blockade, Kupffer cells, liposome, metabolic glycan labeling, cell-free DNA, exosome

1 Introduction

Nanocarriers play an increasingly vital role in modern therapeutics and diagnostics, enabling efficient delivery of diverse cargoes—from small-molecule drugs and imaging agents to nucleic acid-based therapeutics [1-3]. Nanocarriers have also significantly advanced chemical biology research. A prominent example was liposome-assisted metabolic glycan labeling or liposome-assisted bioorthogonal reporter (LABOR), which offers enhanced cell and tissue selectivity for visualization and profiling of glycans [4-7]. However, one major challenge faced by nanocarriers is the rapid clearance by the mononuclear phagocyte system (MPS) in vivo, resulting in typically less than 1% of the injected dose reaching the target tissue [8]. The MPS comprises tissue-resident macrophages, blood monocytes, dendritic cells, and progenitor cells [9]. In the MPS, Kupffer cells account for 80–90% of the body's total macrophage population and are located at the luminal side in the hepatic sinusoid [10, 11]. Based on their strategic location and abundance, Kupffer cells are considered to play a dominant role in sequestering and clearance of circulating nanoparticles. Beyond markedly reducing the circulation half-life and therapeutic efficacy of

exogenously administered nanoparticles, the MPS also actively clears endogenous circulating particles, including nucleosomes [12] and extracellular vesicles [13], thereby undermining the sensitivity of liquid biopsies that rely on biomarkers such as cell-free DNA (cfDNA) or exosomes.

Several strategies have been explored to temporarily attenuate MPS-mediated clearance [14]. These include macrophage depletion with cytotoxic compounds such as clodronate or propamidine in liposomal formulations [15]. Gadolinium chloride was also employed for depletion mainly by suppressing phagocytosis in Kupffer cells [16]. Several compounds negatively impacting endocytosis or lysosome trafficking were also reported to reduce uptake of nanoparticles by MPS [17, 18]. However, systemic and immune-related toxicity concerns were raised for these methods [14]. An alternative and potentially safer strategy was preconditioning of MPS with endogenously induced or exogenously administrated particles, which lower the dose threshold needed for efficient nanocarrier delivery [19]. As an example, hijacking the fact that aged red blood cells (RBCs) are eliminated by MPS, anti-RBC antibodies intensifying this process have been shown to induce the MPS

blockade [20]. Administration of various blank nanoparticles including ferrihydrite [21] or intralipid [22] for temporary and reverse macrophage saturation have proven useful as well.

Among nanoparticles explored for MPS blockade, liposomes have attracted great attention owing to their safety profiles, history of clinical success and formulation flexibility. Beyond augmenting nanoparticle drug delivery [23], liposomes have been shown to reduce cfDNA clearance [24] and improve efficiency of nucleic acid therapeutics such as siRNA and mRNA [25], highlighting the potential of liposomal MPS blockade. Of note, accumulating evidence underscores that the intrinsic biophysical properties of nanocarriers may play a critical role in determining their pharmacokinetics, such as cellular interactions, clearance by the MPS, and in vivo biodistribution [26-29]. However, the screening of effective liposomal MPS blockers along with efforts to elucidate how their formulation dictates MPS uptake efficiency remains rare.

Here, we designed a library of 18 liposomes with systematically varied compositions, and identified a candidate liposomal MPS Blocker through an integrated screening strategy combining in vitro Kupffer cell uptake assays with in vivo biodistribution profiling. Upon simultaneous intravenous injection (i.v.) administration at equal concentration, the liposomal Blocker extended the serum half-life of a widely used FDA‑approved PEGylated liposomal formulation (the carrier in LipoDox®) by 2.1 folds. This Blocker was applied to enhance LABOR in a mouse tumor model. Furthermore, administration of the liposomal Blocker significantly reduced the clearance of circulating biomarkers, including cfDNA and exosomes, in mice. Notably, the use of the MPS Blocker led to a 6.8‑fold increase in recovered cfDNA. Collectively, the identified liposomal MPS Blocker showed potential as a versatile platform for improving nanocarrier-based labeling, therapeutic delivery, as well as circulating biomarker detection.

2 Experimental

2.1 Materials

1,2-Dioleoyl-sn-glycero-3-phosphocholine (DOPC, Cas no. 4235-95-4), 1,2-Distearoyl-sn-glycero-3-phosphocholine (DSPC, Cas no. 816-94-4) and 10 × anticoagulant EDTA solution (catalogue no. A885473) were purchased from Shanghai Macklin Biochemical. Cholesterol (Chol, Cas no. 57-88-25) and 1,2-distearoyl-sn-glycero-3-phosphoethanolamine-N-[methoxy-(polyethylene glycol)-2000] (DSPE-PEG2000, Cas no. 147867-65-0) were purchased from A.V.T. Pharmaceutical Corporation. 2-[4-{(bis[(1-tert-butyl-1H-1,2,3-triazol-4-yl)methyl]amino)methyl}-1H-1,2,3-triazol-1-yl]acetic acid (BTTAA, Cas no. 1334179-85-9) and alkyne-Cy5 (catalogue no. CCTTA116) were purchased from Click Chemistry Tools. Copper (II) sulfate pentahydrate (CuSO$_4$, Cas no. 7758-98-7),), DNase I (catalogue no. D5025) and collagenase (catalogue no. C2674) were purchased from Sigma Aldrich. Sodium-L-ascorbate (catalogue no. S105026) was purchased from Aladdin. Sulfo-Cy5-COOH (catalogue no. S61728), Sulfo-Cy3-COOH (catalogue no. S25252) and Sephadex G-50

(catalogue no. S14032) were purchased from Yuanye Bio-Technology. Polycarbonate membrane (catalogue no. 800282 and 800281) was purchased from Whatman. 9AzSia was synthesized as previously described [30].

Immortalized mouse Kupffer cells (catalogue no. BNCC340733) were purchased from BeNa culture collection. Mouse Kupffer cell complete medium (catalogue no. CM-M132) was purchased from Wuhan Procell Life Science & Technology. Dulbecco modified eagle medium (DMEM, catalogue no. 11965092), USA fetal bovine serum (FBS, catalogue no. A5669701) and Penicillin-Streptomycin (10,000 U/mL, catalogue no. 15140122) were acquired from Gibco Life Sciences. Tissue-Tek O.C.T. compound (catalogue no. 4583) was purchased from Sakura. FITC-conjugated anti-mouse F4/80 antibody (catalogue no. 123107) was purchased from Biolegend. Hoechst 33342 (catalogue no. IH00702) was purchased from Solarbio. DBCO-Cy5 (catalogue no. #923) was purchased from AAT Bioquest. Apostle MiniMax high efficiency cfDNA isolation kit (catalogue no. A17830) was purchased from Apostle Bio. PowerUp™ SYBR™ green master Mix (catalogue no. A25742) was purchased from Thermo Fisher Scientific. BeyoMag™ blood genomic DNA isolation kit with magnetic beads (catalogue no. D0091S), carrier RNA (catalogue no. R0036), 4% paraformaldehyde (PFA, catalogue no. P0099) and QuickBlock blocking buffer (catalogue no. P0252) were purchased from Beyotime. Exosomes affinity-based isolation kit (EVlent™, catalogue no. EV02-05-01) was purchased from EVLiXiR. CD9 antibody (catalogue no. HY-P80610) was purchased from Medchem Express. anti-rabbit IgG, HRP-linked antibody (HRP anti-rabbit antibody, catalogue no. 7074S) was purchased from Cell Signaling Technology. SDS-PAGE loading buffer (catalogue no. WB2001) was purchased from New Cell & Molecular Biotech. Polyvinylidene fluoride (PVDF) membrane (catalogue no. IPVH00010) and Immobilon Western Chemiluminescent HRP Substrate (catalogue no. WBKLS0500) were purchased from Merck Millipore. All primers were purchased from RuiBiotech.

2.2 Liposome Preparation and Characterization

Liposomal blocker candidates were prepared by a thin-film hydration–extrusion method. Lipid mixtures containing DOPC, DSPC and Chol at different molar ratios were dissolved in chloroform, and the solvent was evaporated in a round-bottom flask to yield a uniform lipid film that was further dried under vacuum overnight. The lipid film was rehydrated at room temperature with PBS (pH 7.4) or PBS containing 2.5 mM sulfo-Cy5-COOH. After 10 min sonication, the dispersion underwent ten freeze–thaw cycles using liquid nitrogen and bath at 37 °C. The resulting multilamellar vesicles were then extruded 21 times through a polycarbonate membrane with a pore size of 0.4 μm, and free Sulfo-Cy5-COOH was removed on a Sephadex G-50 column.

Phospholipid content was determined using the Stewart assay. Liposomes (LPs) were diluted 100-fold with chloroform and mixed with ammonium ferrithiocyanate reagent to form a colored complex. The chloroform layer was then collected and its absorbance was measured at 488 nm using a UV photometer.

The concentration of encapsulated Sulfo-Cy5-COOH

within liposomes was measured by fluorescence intensity (λex 650 nm, λem 670 nm) on a Synergy 4 microplate reader (BioTek, USA) subsequent to the complete disruption of liposomes using 0.1% (v/v) Triton X-100. The liposome diameters were measured via dynamic light scattering (DLS, Brookhaven ZetaPALS instrument).

Carrier was prepared following the same protocol, except for being rehydrated with 2.5 mM Sulfo-Cy3-COOH or 9AzSia aqueous solutions (300 mM) before extruded through 0.2-μm polycarbonate membranes to obtain carrier-Cy3 and carrier-9Az, respectively.

2.3 Cell culture and in vitro liposomal uptake screening.

Kupffer cells were cultured in mouse Kupffer cell complete medium. 4T1 cells were cultured in DMEM containing 10% fetal bovine serum (FBS) supplemented with 100 units/mL penicillin and 100 μg/mL streptomycin (p/s). For liposome screening in vitro, Kupffer cells were seeded at 4.0×10^5 cells/mL in 6-well plates and were allowed to adhere for 12 h. Subsequently, Sulfo-Cy5-encapsulated LPs were added to the designated wells at a final Cy5 concentration of 1 μM. Following a 3 h incubation, the cells were washed three times with PBS to remove unbound liposomes. Cellular uptake was then quantified by measuring Cy5 fluorescence via flow cytometry.

2.4 Animals

6-8-week-old BALB/c female mice were purchased from Vital River Laboratory Animal Center and maintained under specific pathogen–free conditions.

2.5 Characterization of liposome distribution in mice

Guided by the in vitro screening data, we selected the three LP formulations exhibiting the highest Kupffer cell uptake capacity (DOPC: DSPC: Chol = 10:0:5, 8:2:10 and 10:0:10) for LP blockers screening in vivo. Mice were administered with each of the three LPs via tail vein at a dose of 1.2 μmol/kg Cy5-equivalent. Various tissues (liver, heart, spleen, lung and kidney) were harvested for ex vivo imaging 30 min post-treatment, using a Perkin-Elmer IVIS animal imaging system. Additionally, mouse liver tissues were also collected and fixed with 4% paraformaldehyde (PFA) at 4 °C overnight followed by dehydration with 15% sucrose and 30% sucrose for at least 48 h. The tissues were then embedded with Tissue-Tek O.C.T. compound and sectioned at 10 μm thickness on a cryostat (Leica CM1950) at -20 °C. The liver sections were incubated with 5 μg/mL of FITC-conjugated anti-mouse F4/80 antibody at 4 °C overnight, then washed with PBS for three times and stained with Hoechst 33342 (5 μg/mL) for an additional 2 h, followed by fluorescence microscopy analysis on a Zeiss LSM 700 confocal laser scanning microscope (CLSM).

2.6 Liposomal MPS blockade

To investigate the impact of the Blocker/Carrier ratio on liposomal MPS blockade effects, the Blocker dose was fixed at 0.2 mmol/kg lipid, while the Carrier-Cy3 dose was varied at 0.1, 0.2, or 0.4 mmol/kg. Mice were co-administered with both Blocker and Carrier via tail-vein injection, with Carrier-Cy3 alone serving as the control group. Tissues (liver, heart, spleen, lung and kidney) were harvested 30 minutes post-injection and imaged ex vivo using a PerkinElmer IVIS imaging system.

2.7 Pharmacokinetics

For the pharmacokinetics study, mice were co-administered with both Carrier-Cy3 (0.2 mmol/kg lipid) and Blocker (0.2 mmol/kg lipid) via tail vein, with Carrier-Cy3 alone serving as the control group (No Blocker). At predetermined time points, blood was sampled from the retro-orbital sinus of mice using non-heparinized capillary tubes. After clotting at room temperature for 30 min, the blood samples were centrifuged at 2,000g for 10 min at 4 °C, and serum was carefully transferred to fresh tubes. Liposomes in serum were completely lysed with 0.1 % Triton X-100, and the half-life of Carrier was determined from Cy3 absorbance measurements at 550 nm using a Synergy 4 microplate reader (Bio-Tek, USA).

2.8 Metabolic glycan labeling

Subcutaneous 4T1 breast tumors were established in 6-week-old female BALB/c mice by inoculating 1×10^6 4T1 cells into the right flank. When tumors reached ~200 mm³, mice were randomized into two groups and treated intravenously with either (i) Carrier-9AzSia alone (0.2 mmol/kg lipid, No Blocker) or (ii) the mixture of Blocker (0.2 mmol/kg lipid) and Carrier-9AzSia (0.2 mmol/kg, With Blocker). After 24 h, DBCO-Cy5 was administered intravenously at a dose of 5 mg/kg. At 48 h post-treatment, all mice were subjected to in vivo imaging using a Perkin-Elmer IVIS animal imaging system. Subsequently, tumors were excised and divided into three portions. One portion was cut into small pieces, and then digested with 435 U/ml DNase I and 218 U/ml collagenase in DMEM at 37 °C for 30 min. The digested tissue was passed through a sterile 70 μm cell strainer to remove any undigested debris. The resulting cell suspension was washed three times with ice-cold PBS and resuspended in PBS for flow cytometry analysis. The second portion was homogenized and lysed with 4% (w/v) SDS in PBS. The lysate was sonicated, heated at 95 °C for 10 min, and incubated for 1 h at room temperature in a click buffer containing 100 μM alkyne-Cy5, 50 μM CuSO$_4$, 100 μM BTTAA, and 2.5 mM freshly prepared sodium-L-ascorbate. Following SDS-PAGE, fluorescent bands were visualized using a Typhoon FLA 9500 scanner to quantify Cy5 retention in tumor. Equal loading was assessed by Coomassie staining and ChemiDoc XRS+ imaging. The remaining tumor portion was fixed with 4% PFA at 4 °C overnight, followed by dehydration in 15% sucrose and 30% sucrose for at least 48 h, then embedded in Tissue-Tek O.C.T. compound, snap-frozen, sectioned at 10 μm thickness, and stained with Hoechst 33342 (5 μg/ml) for imaging by confocal microscopy.

2.9 Genomic DNA (gDNA) extraction and quantification

gDNA was extracted from mouse blood using the BeyoMag™ blood genomic DNA isolation kit and quantified on a Qubit fluorometer (Invitrogen). The purified gDNA stock was stored at −20 °C. A standard curve was prepared from serial dilutions of the stock using water with 0.1 % (v/v) Tween-20 to yield gDNA solutions at 0.08, 0.4, and 2 ng/μL concentrations. The freshly prepared dilutions were analyzed by quantitative PCR (qPCR).

2.10 Cell-free DNA extraction (cfDNA) and quantification

Mice were administered via the tail vein injection with (i) PBS, (ii) 100 mg/kg (0.085 mmol/kg lipid) of the Blocker, or (iii) 300 mg/kg (0.256 mmol/kg lipid) of the Blocker. One-

hour post-injection, blood was collected from the retro-orbital sinus into 1.5-mL DNA-free tubes containing 10 × EDTA anticoagulant solution. Samples were immediately placed on ice, and centrifuged at 1000g for 10 min at 4 °C. The plasma was transferred to a fresh 1.5-mL tube and centrifuged again at 3000g for 10 min at 4 °C to remove residual cells.

cfDNA was extracted from plasma using the high efficiency cfDNA isolation kit, and eluted with 12 uL elution buffer containing 20 ng/μL spike-in carrier RNA. For qPCR analysis, 9 μL cfDNA was combined with 10 μL PowerUp™ SYBR™ green master mix, 1 μL primer mixture containing forward primer (5 μM) reverse primer (5 μM). Quantitation was performed on a StepOne Plus Real-Time PCR System (Applied Biosystems). All primers were designed with the NCBI Primer-BLAST tool, and their sequences are listed in Table S2 in the ESM.

Plasma cfDNA concentrations (ng/mL) were quantified using a gDNA-derived calibration curve (Figure S5 in the ESM) generated by linear regression. Sample *Ct* values obtained from qPCR were substituted into the calibration curve to calculate cfDNA concentration c (ng/μL) in the eluate. Total cfDNA yield was then calculated as c × 12 μL (elution volume) and normalized to ng/mL plasma relative to the original plasma volume.

2.11 Exosome extraction and quantification

Plasma was obtained as detailed in cfDNA extraction and quantification, and exosomes were isolated from 200 μL plasma using an exosome affinity-based isolation kit. For western blot analysis, exosome-enriched beads were resuspended in 25 μL of 2 × SDS-PAGE loading buffer and heated at 98 °C for 10 min. The supernatants were collected by magnetic separation and diluted with PBS to 50 μL. Samples were separated by SDS-PAGE and transferred onto PVDF membranes. Membranes were blocked with QuickBlock blocking buffer overnight at 4 °C and incubated with CD9 antibody in TBST overnight at 4 °C. After three washes with TBST, membranes were incubated with HRP-conjugated anti-rabbit secondary antibody in TBST for 1 h at room temperature, followed by three washes with TBST. Protein blots were visualized using Immobilon Western Chemiluminescent HRP Substrate and imaged with a 5200 Chemiluminescence Imaging System (Tanon, China).

3 Results and discussion

3.1 Liposome library preparation and in vitro Kupffer cell uptake screening

Several liposome biophysical properties such as stiffness and fluidity are correlated with the phase transition temperature (Tm). Therefore, aiming to prepare a combinatorial liposome library with varied phase transition temperatures, DOPC (Tm = -17 °C) and DSPC (Tm = 55 °C), two widely used phospholipids with significantly different Tm values were selected as the main component and blended at different molar ratios. Additionally, Chol was incorporated at different percentages to further diversify the library (Figure 1a). A total of 18 liposomes with distinct formulations were successfully prepared by a thin-film hydration–extrusion method, with varied molar ratios of DOPC: DSPC: Chol (Figure 1b). The liposomes were organized into three groups, with (DOPC + DSPC): Chol molar ratios being 10:3, 10:5, and 10:10, respectively. Within each group, the molar ratio of DOPC to DSPC varied from 0:10 to 10:0. DLS analysis confirmed that all liposomes exhibited hydrodynamic diameters ranging from approximately 220 nm to 300 nm, with polydispersity indices between 0.1 and 0.2 (Table S1 in the ESM), indicating high uniformity across the library.
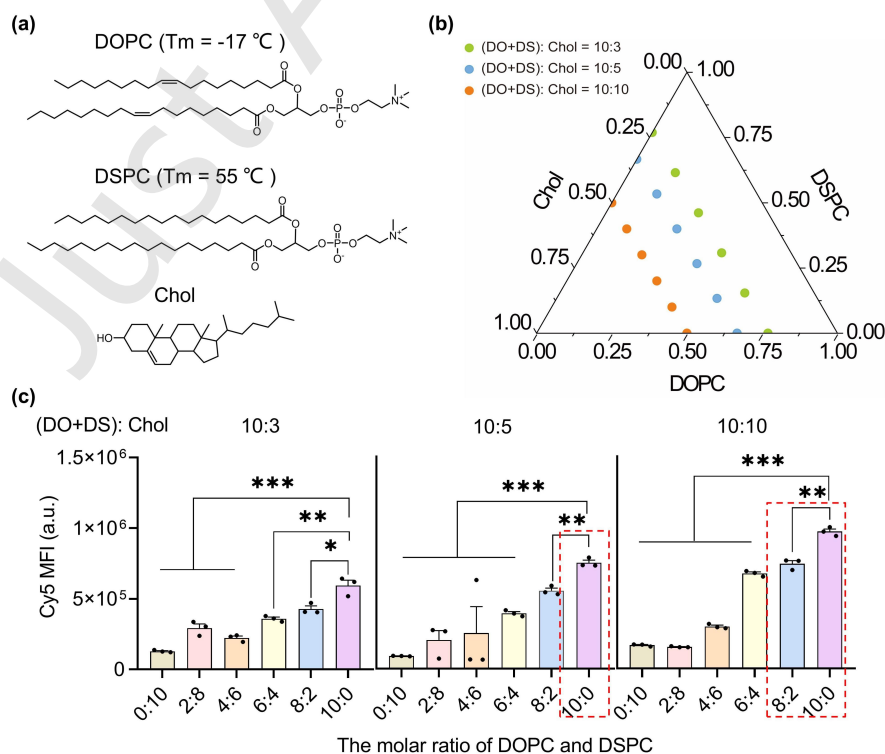

Figure 1 Design, preparation and Kupffer cell uptake screening of a combinatorial liposome library for mononuclear phagocyte system blockade. (a) Chemical structures of DOPC, DSPC and Chol which were mixed at different molar ratios for the preparation of 18 different liposomes (LPs). (b)

Ternary phase diagram showing the relative proportions of DOPC, DSPC, and Chol in each formulation of the LP. (c) Flow cytometry analysis of Kupffer cell liposomal uptake. Kupffer cells were treated with various LPs-Cy5 for 3 h before analysis. The three LPs showing the highest Kupffer cell uptake were highlighted in red dashed frame. Data represent mean ± SEM from three biological replicates. P values were calculated by one-way ANOVA. a.u. arbitrary units. *P < 0.05; **P < 0.01; ***P < 0.001.

Liposomes encapsulating Cy5 (LPs-Cy5) were prepared to dissect MPS uptake efficiency for the 18 candidates. The encapsulated Cy5 concentrations were listed in Table S2 in the ESM. Immortalized mouse Kupffer cells (ImKC) were treated with various LPs-Cy5 (1 μM based on Cy5) for 3 h at 37 °C, followed by washing and flow cytometry analysis to quantify Kupffer cell uptake (Figure 1c). Within each group with fixed (DOPC + DSPC): Chol molar ratio, the Cy5 mean fluorescence intensity (MFI) was significantly different and a generally increasing trend was observed as the molar ratio of DOPC/DSPC increased, suggesting a favored uptake of low-Tm liposome by Kupffer cells. Additionally, cholesterol titration from 23.1 to 50 mol% elicited only a modest uptick in LPs internalization. These results confirmed that the Kupffer cell-liposome interactions and subsequent uptake efficiencies were correlated with intrinsic liposomal biophysical properties. Based on the in vitro results, three liposome formulations showing the highest uptake signal (as indicated by the red dashed boxes in Figure 1c) corresponding to the formulations of (DOPC+DSPC): Chol = (10+0):5, (8+2):10, and (10+0):10, were selected for subsequent in vivo screening and bio-distribution analysis.

3.2 In vivo liposomal MPS blocker screening and characterization

To identify the optimal liposomal Blocker formulation from the three candidates, BALB/c mice were i.v. administered with each of the three LPs-Cy5 (1.2 μmol/kg based on Cy5). Various tissues were harvested for ex vivo imaging 30 min post-injection. This short interval was chosen to mainly reflect the intrinsic MPS uptake and minimize other contributions such as clearance. Ex vivo imaging revealed distinct accumulation profiles across the three formulations (Figure 2a). The highest Cy5 fluorescence intensity was observed in mice treated with the (DOPC+DSPC): Chol = (10+0):10 formulation (Figure 2b). Quantitative analysis showed that the hepatic Cy5 intensity in this group was 1.6‑fold and 1.9‑fold higher than the other two groups, respectively. To further analyze the distribution and cellular targeting of the liposomes in liver, liver sections were immunostained with FITC‑conjugated F4/80 antibody and examined by CLSM (Figure 2c). The Cy5 signal showed extensive overlap with F4/80‑positive Kupffer cells, with minimal localization to hepatocytes or sinusoidal endothelial cells. These results collectively establish the formulation DOPC: Chol = 50:50 as the optimal candidate for MPS blockade, which we refer to as the "Blocker."
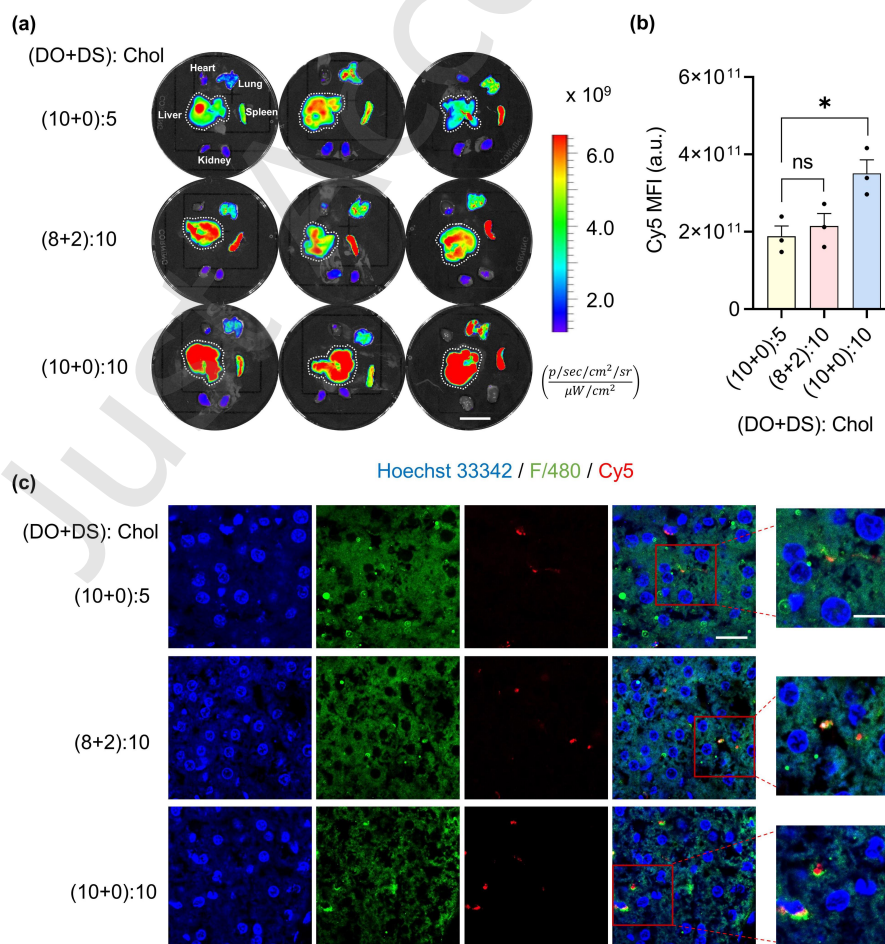

Figure 2 Biodistribution analysis of candidate liposomal blockers in mice. (a) Ex vivo fluorescence imaging showing the distribution of the three selected LPs-Cy5 in major organs of BALB/c mice. Mice were i.v. administered with each LP-Cy5 (1.2 μmol/kg based on Cy5) and sacrificed 0.5 h post

treatment. Liver was highlighted by dashed circle. Three biological replicates were performed for each group. Scale bar, 2 cm. (b) Quantified fluorescence intensity of Cy5 signal in liver. Data represent mean ± SEM from three biological replicates. *P* values were calculated by one-way ANOVA. a.u. arbitrary units. *P < 0.05; ns not significant. (c) Representative CLSM images of frozen liver sections from mice treated as described in (a). The sections were immunostained with FITC labeled F4/80 antibody and stained with Hoechst 33342. Scale bars, 10 μm and 20 μm for zoomed-in and zoomed-out images, respectively.

To functionally validate the efficacy of the identified Blocker, we performed a competitive assay by co-administering it with a widely used liposomal carrier. The objective was to determine whether the Blocker could reduce MPS-mediated clearance and prolong the systemic circulation of a co-injected nanocarrier. Of note, the co-administration of blocker and carrier, while more convenient, is also more challenging than pre-treatment with blocker followed by carrier injection, which was commonly used in previous efforts in MPS blockade development [14]. As a representative nanocarrier, the liposome in Lipodox® (Sun Pharmaceutical Industries Ltd, DSPC: Chol: DSPE-PEG2000 = 56:39:5) [31, 32], an FDA‑approved PEGylated liposome was selected and was hereafter referred to as "Carrier". The Carrier was prepared using a conventional thin-film hydration and extrusion method. A side-by-side comparison of the Blocker and Carrier liposomes was summarized in Figure 3a. The Carrier had a mean hydrodynamic diameter of 184.1 ± 1.4 nm, which was comparable to that of the Blocker (224.0 ± 2.7 nm). DSPC was the main lipid component in the widely used efficient nanocarrier. This was aligned well with our in vitro screening results showing that DSPC-rich formulations were less efficiently internalized by Kupffer cells (Figure 1), which

was desired for efficient in vivo delivery. Furthermore, the presence of PEGylation on the Carrier surface helps to minimize opsonization, aggregation, and phagocytic uptake, thereby favoring extended circulation [33].

For the competition assay, the mice were intravenously injected with mixtures of Cy3-labeled Carrier (Carrier-Cy3; 0.1, 0.2, or 0.4 mmol/kg, respectively based on lipid) and the Blocker (fixed at 0.2 mmol/kg lipid). In control experiments, the mice were administrated with Carrier-Cy3 alone. Tissues were harvested at 0.5 h post-injection for ex vivo imaging (Figure 3b). A marked reduction in hepatic Cy3 MFI was observed in the "With Blocker group" compared to controls (Figure 3c, d). The MFI values in the presence of Blocker were 65.9%, 52.1%, and 74.2% of those in the control group at three different Carrier dosages, respectively, suggesting ratio-related MPS blocking effects. Pharmacokinetic analysis further confirmed the functional benefit of Blocker co-administration at equal concentration (Figure 3e). The circulation half-life ($t_{1/2}$) of the Carrier was extended from 1.1 h without Blocker to 2.3 h when co-administrated with Blocker at equal concentration, representing a 2.1-fold increase and confirming a significant prolongation of systemic exposure.
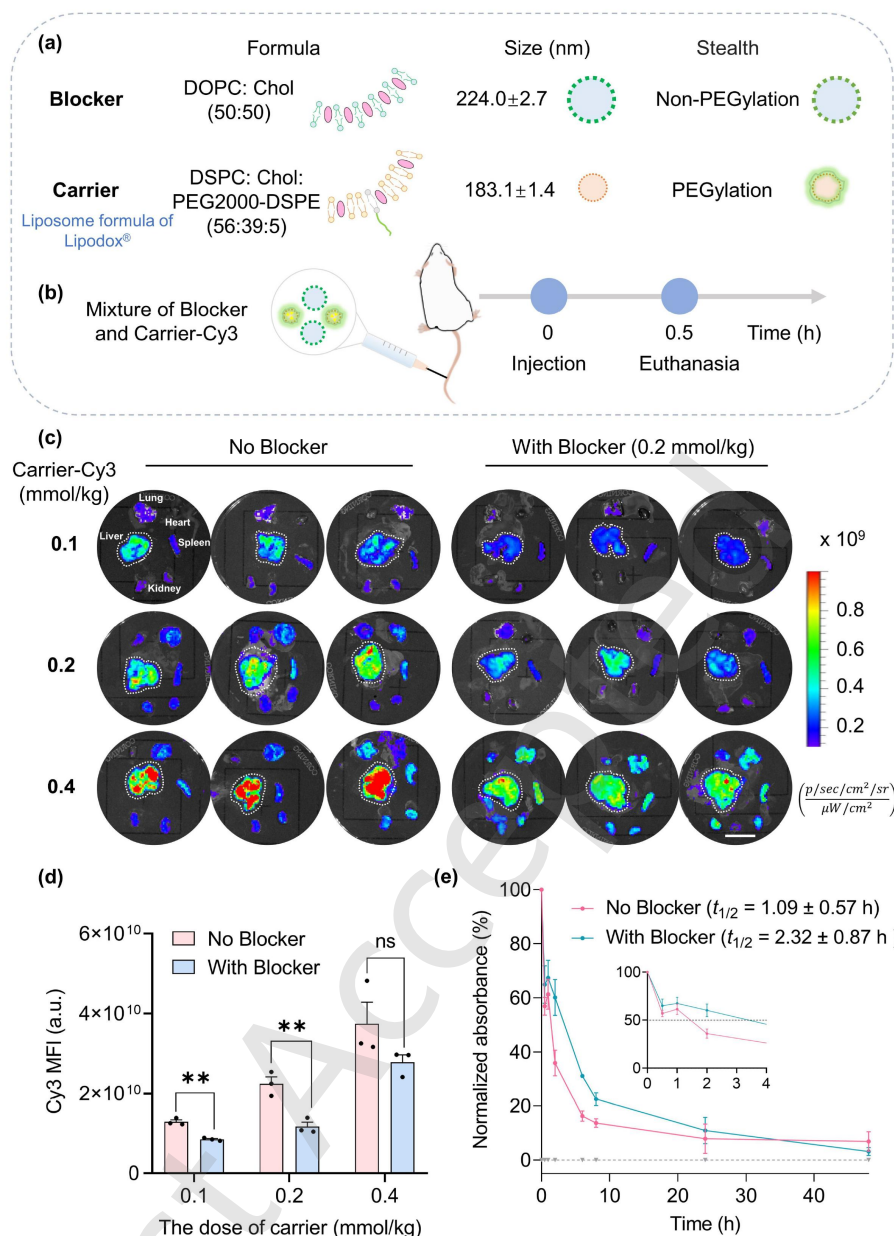
Figure 3 In vivo assessment of liposomal MPS blockade. (a) Schematic diagram comparing liposomal Blocker and Carrier in terms of formulation, size and stealth. (b) Schematic of experimental procedures for biodistribution analysis of Carrier-Cy3 with or without Blocker. BALB/c mice were i.v. administrated with the mixture of Blocker and Carrier-Cy3. The mice were then euthanized 0.5 h post-injection, and their tissues were isolated for ex vivo imaging, Carrier alone without Blocker was used as the control. (c) Ex-vivo fluorescence imaging of various organs following the procedure in (b). Liver was highlighted by a dashed circle. Three biological replicates were performed for each group. Scale bar, 2 cm. (d) Quantified fluorescence intensity of Cy3 in the liver. Data represent mean ± SEM from three biological replicates. *P* values were calculated by one-way ANOVA. a.u. arbitrary units. **$P < 0.01$; *ns* not significant. (e) Pharmacokinetic profiles and half-life ($t_{1/2}$) analysis of Carrier-Cy3 in mice serum with or without Blocker at equal concentration. Data represent mean ± SEM from three biological replicates.

To exclude the possibility that the observed effects were due to a non-specific dose-saturation effect, Carrier-Cy3 (0.2 mmol/kg lipid) was co-injected with empty Carrier at equal concentration. No significant difference in liver fluorescence was detected between this group and the Carrier-Cy3-only group (Figure S1 in the ESM), confirming that the MPS blockade effect should be attributed to the optimized formulation of the Blocker and not merely an increase in total lipid dose. Collectively, these results suggest that the Blocker should be preferentially taken up by Kupffer cells, thereby competitively inhibiting MPS clearance of a co-administered nanocarrier.

3.3 Liposomal MPS blocker for enhanced liposome-assisted

metabolic glycan labeling

We next evaluated the effect of liposomal MPS blockade on metabolic glycan labeling in vivo using liposomes encapsulating azido sugars (Figure 4a). BALB/c mice bearing subcutaneous 4T1 tumors were divided into two groups: the first group (With Blocker group) were co-administrated intravenously with Blocker (0.2 mmol/kg lipid) and 9AzSia-encapsulated Carrier (Carrier-9AzSia, 0.2 mmol/kg lipid), while the control group (No Blocker) received Carrier-9AzSia alone. DBCO-Cy5 was administered intravenously 24 h post liposome injection, to label azide-modified sialoglycans via copper-free click chemistry [34]. After another 24 h, the mice were anesthetized prior to in vivo

imaging to visualize the labeled sialoglycans. A markedly enhanced glycan labeling signal in tumor region was observed in the "With Blocker group" (Figure 4b). Quantitative analysis confirmed that the Cy5 MFI values in

tumor region of the "With Blocker group" were significantly higher than those in the control group, with a 1.7-fold enhancement (Figure 4c).
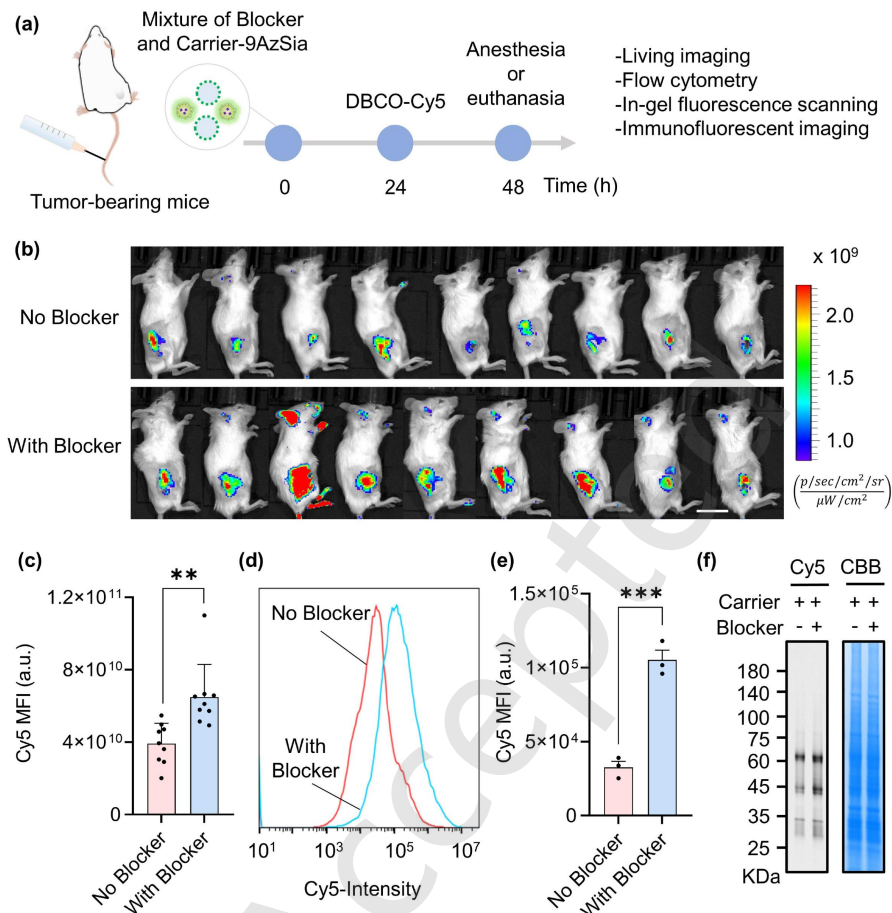

Figure 4 MPS blockade for enhanced liposome-assisted metabolic glycan labeling in vivo. (a) Schematic of experimental procedures for liposomal-assisted metabolic glycan labeling with or without liposomal Blocker. A mixture of liposome Blocker and Carrier-9AzSia was i.v. administrated into 4T1 tumor-bearing BALB/c mice at 0 h, and DBCO-Cy5 was administered at 24 h. Mice were anesthetized at 48 h for living imaging, followed by euthanasia to collect the tumor. Carrier alone without Blocker was used as the control. (b) In vivo whole-body fluorescence imaging of mice. Nine biological replicates were performed for each group. Scale bar, 2 cm. (c) Quantified fluorescence intensity of Cy5 in tumor region. Data represent mean ± SEM from nine biological replicates. P values were calculated by one-way ANOVA. **P < 0.01. ((d) and (e)) Representative flow cytometry analysis of single cell suspension obtained from tumor tissue dissociation (d) and their quantitation of Cy5 fluorescence intensity (e). In (e), data represent mean ± SEM from three biological replicates. P values were calculated by one-way ANOVA. ***P < 0.001. (f) Representative in-gel fluorescence scanning of tumor lysates after reaction with alkyne-Cy5. The Coomassie Brilliant Blue (CBB)-stained gel demonstrates comparable protein loading across samples. Five biological replicates were performed. Full results for the five replicates and fluorescence intensity statistical analysis were presented in Figure S3 in the ESM.

To further assess labeling efficiency at the cellular level, the mice were euthanized and single-cell suspensions derived from dissociated tumor tissues were analyzed by flow cytometry (Figure 4d, e). A 3.2-fold increase in Cy5 signal intensity was observed in the "With Blocker group" compared to controls. Consistent with these findings, CLSM imaging of tumor tissue sections exhibited stronger Cy5 fluorescence in the presence of Blocker (Figure S2 in the ESM). To compare the efficiency of liposome-mediated incorporation of 9AzSia into tumor sialylated glycoproteins, the tumor lysates were reacted with alkyne-Cy5 via copper(I)-catalyzed alkyne-azide cycloaddition (CuAAC) [35] before in-gel fluorescence scanning analysis, which demonstrated enhanced the labeling intensity with Blocker (Figure 4f and Figure S3 in the ESM). Collectively, these data indicate that liposomal MPS blockade effectively improves

liposome-mediated metabolic glycan labeling, presumably by prolonging the systemic circulation of the liposome carrier encapsulating unnatural sugars and thus enhancing tumor accumulation.

3.4 Liposomal MPS Blocker for increased circulating biomarker recovery

Liquid biopsy analyzing biomarkers such as cfDNA and exosomes has emerged as a promising non-invasive approach for diagnosis and disease monitoring. Both cfDNA and exosomes are rapidly cleared from circulation by the MPS, which substantially compromises their detection sensitivity and clinical utility. We anticipated that the liposomal MPS Blocker developed in this study may enhance the recovery of these biomarkers, thereby improving the performance of liquid biopsy in clinical settings (Figure 5a).
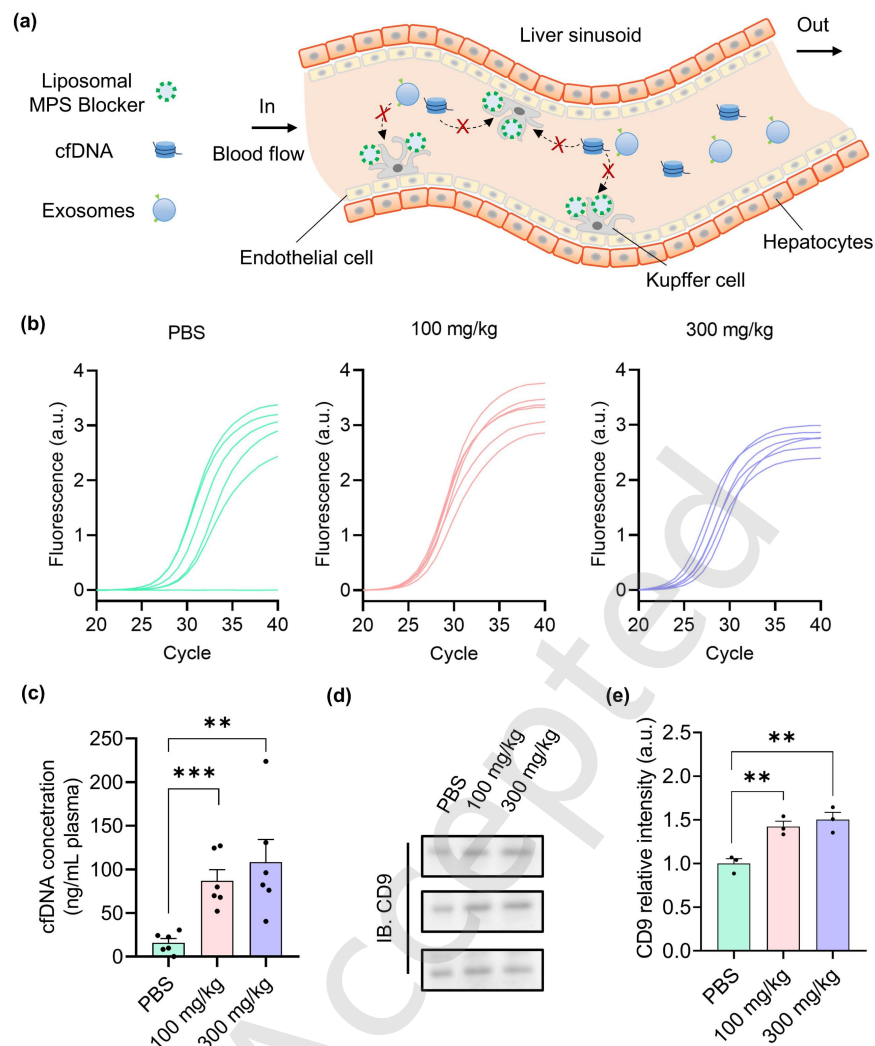
Figure 5 MPS blockade for reduced clearance of cfDNA and exosome. (a) Schematic for MPS Blocker-mediated enhancement of circulating biomarkers recovery. (b) The qPCR amplification curves of plasma cfDNA samples from mice treated with PBS, 100 mg/kg (0.085 mmol/kg) Blocker or 300 mg/kg (0.256 mmol/kg) Blocker 1 h before plasma collection. Six biological replicates were performed for each group. (c) Quantified cfDNA yield from mice plasma. Data represent mean ± SEM from six biological replicates. P values were calculated by one-way ANOVA. **$P < 0.01$; ***$P < 0.001$. (d) Western blotting analysis of exosomes extracted from plasma samples. Exosome-specific marker CD9 was used to reflect the exosome concentration. Three biological replicates were performed for each group. (e) Quantified relative intensity from the western blot analysis. Data represent mean ± SEM from three biological replicates. P values were calculated by one-way ANOVA. **$P < 0.01$.

To test whether liposomal MPS blockade could inhibit the clearance of cfDNA and exosomes in vivo, mice were i.v. administrated with PBS, low dose Blocker (100 mg/kg), and high dose Blocker (300 mg/kg), respectively. After one hour, 200 μL plasma sample was collected from each mouse for cfDNA and exosome extraction. A pair of primer covering a 101-bp amplicon in mouse genome (Table S3 in the ESM) was used in qPCR to compare the amount of cfDNA. As shown in Figure 5b, qPCR amplification curves for cfDNA samples extracted from Blocker-treated mice exhibited a marked shift to left side as compared to PBS group, corresponding to smaller cycle threshold (Ct) and higher cfDNA concentration due to MPS blockade. To quantify cfDNA concentrations, a standard curve was generated using mouse genomic DNA (gDNA) of known concentrations (Figures S4 and S5 in the ESM). Based on the standard curve and the Ct values, the amounts of amplifiable cfDNA were calculated. The Blocker treatment led to a 5.5-fold and 6.8-fold increase in mean cfDNA recovery at 100 mg/kg and 300 mg/kg doses, respectively, compared to the PBS control

(Figure 5c). Exosomes isolated from the plasma samples were analyzed by western blot, using the signal from exosome-specific marker CD9 to reflect the exosome concentration. As shown in Figure 5d, stronger CD9 band intensities were observed in both Blocker-treated groups than the PBS group. Statistical analysis confirmed a significant increase in CD9 signal comparing to PBS control ($P < 0.01$), with 1.4-fold and 1.5-fold enhancements at 100 mg/kg and 300 mg/kg, respectively (Figure 5e). These results demonstrate improved isolation yield for both circulating biomarkers by the Blocker.

4 Conclusions

The efficient delivery of nanocarriers and sensitive detection of circulating biomarkers are significantly hampered by their rapid clearance by the MPS. To overcome this limitation, we constructed a liposomal library with various formulations and identified a potent MPS-blocking liposome (the Blocker) through an integrated screening strategy combining in vitro Kupffer cell uptake assays with

in vivo biodistribution profiling. Upon co-administration at equal concentration, the Blocker effectively competed for MPS uptake, extending the circulation half-life of a co-injected PEGylated liposomal Carrier by 2.1 folds. Theoretically, co-administration presents a greater challenge than a pre-conditioning protocol using the same Blocker, due to the lack of the time window for the Blocker to act before the Carrier is introduced. The fact that the Blocker effectively extended the circulation half-life of a widely used liposomal Carrier even under this stringent co-administration setting provides strong validation of its blocking efficiency. We therefore anticipate that the Blocker would perform with equal or even higher efficiency in a pre-conditioning protocol.

This MPS blockade strategy, in combination with liposome carriers encapsulating azido sugars, significantly enhanced tumor-selective metabolic glycan labeling in mice. Furthermore, the Blocker markedly inhibited the clearance of mice endogenous circulating biomarkers, leading to a 6.8-fold increase in recovered cfDNA and enhanced exosome recovery. As evidenced by the efficient improvement for both nanocarrier delivery and circulating biomarker detection, the liposomal Blocker may represent a versatile platform with broad potential to advance a range of biomedical applications. Given the reported low toxicity of both cfDNA with extended circulation [24] and nanoparticles with plasma half-lives reaching 16.6 h [36] or even exceeding 20 h [37], we anticipate overall low safety concerns regarding the prolonged circulation of both endogenous and administered particles in mice. One important future direction would be to systematically and rigorously evaluate the safety profile and efficacy of MPS Blocker across diverse animal models and, ultimately, in clinical settings.

The more substantial increase in cfDNA yield compared to exosomes following MPS blockade might be due to the differences in their clearance kinetics and the detailed mechanisms by which they are recognized and cleared. While the circulation half-life of cfDNA was reported to be around 16 minutes [38] to 2 hours [39], the clearance of exosomes was more rapid, with a half-life of only 2-7 minutes [40, 41]. The shorter half-life indicates a higher baseline clearance rate and a greater challenge for complete MPS blockade. Furthermore, circulating nucleosome-bound cfDNA exists as compact nucleoprotein complexes with a diameter typically in the range of 10-20 nm [42], while exosome is extracellular vesicle with a diameter ranging from 30 to 150 nm [43]. The distinct physical properties of the two biomarkers could lead to differential competition with the liposomal Blocker used in this work. Despite differential Blocker-derived improvement between cfDNA and exosomes, the Blocker's ability to enhance the yield of both highlights its potential to improve the detection of other biomarkers. Further studies extending this approach to other rapidly cleared targets, such as circulating tumor cells (CTCs) and apoptotic bodies, are warranted and may validate its utility as a universal pre-analytical enhancer for liquid biopsy.

Electronic Supplementary Material: Supplementary

material (Tables S1-S3 and Figures S1–S5) is available in the online version of this article at https://doi.org/10.26599/NR.2026.94908501.

Data availability

All data needed to support the conclusions in the paper are presented in the manuscript and the Electronic Supplementary Material. Additional data related to this paper may be requested from the corresponding author upon request.

Acknowledgements

Declaration of competing interest

All the contributing authors report no conflict of interests in this work.

Author contribution statement

P. F.: Experimental design, investigation, methodology, visualization, and writing original draft. T. Z.: Experimental design and investigation. R. H., L.G. and G. H.: Help with investigation. X. C.: Conceptualization, project administration, data analysis and writing manuscript. P. D.: Conceptualization, project administration, experimental design, data analysis and writing manuscript. All authors have approved the final manuscript.

Informed consent

Not applicable.

Ethics statement

All animal experiments were performed in accordance with guidelines approved by the Institutional Animal Care and Use Committee of Peking University (IACUC protocol number: CCME-ChenX-3) accredited by the Association for Assessment and Accreditation of Laboratory Animal Care (AAALAC) International.

Use of AI statement

None.

References

[1]   Shi, J.; Kantoff, P. W.; Wooster, R.; Farokhzad, O. C., Cancer nanomedicine: progress, challenges and opportunities. *Nat. Rev. Cancer* 2017, 17 (1), 20-37.
[2]   Chen, G.; Roy, I.; Yang, C.; Prasad, P. N., Nanochemistry and Nanomedicine for Nanoparticle-based Diagnostics and Therapy. *Chem. Rev.* 2016, 116 (5), 2826-85.
[3]   Huang, X.; Kong, N.; Zhang, X.; Cao, Y.; Langer, R.; Tao, W., The landscape of mRNA nanomedicine. *Nat. Med.* 2022, 28 (11), 2273-87.
[4]   Xie, R.; Hong, S.; Feng, L.; Rong, J.; Chen, X., Cell-Selective Metabolic Glycan Labeling Based on Ligand-Targeted Liposomes. *J. Am. Chem. Soc.* 2012, 134 (24), 9914-17.
[5]   Xie, R.; Dong, L.; Du, Y.; Zhu, Y.; Hua, R.; Zhang, C.; Chen, X., In vivo metabolic labeling of sialoglycans in the mouse brain by using a liposome-assisted bioorthogonal reporter strategy. *Proc. Natl. Acad. Sci. U.S.A.* 2016, 113 (19), 5173-78.
[6]   Sun, Y.; Hong, S.; Xie, R.; Huang, R.; Lei, R.; Cheng, B.; Sun, D.-e.; Du, Y.; Nycholat, C. M.; Paulson, J. C.; Chen, X., Mechanistic

Investigation and Multiplexing of Liposome-Assisted Metabolic Glycan Labeling. *J. Am. Chem. Soc.* 2018, 140 (10), 3592-602.

[7] Xie, R.; Dong, L.; Huang, R.; Hong, S.; Lei, R.; Chen, X., Targeted Imaging and Proteomic Analysis of Tumor-Associated Glycans in Living Animals. *Angew. Chem. Int. Ed.* 2014, 53 (51), 14082-86.

[8] Wilhelm, S.; Tavares, A. J.; Dai, Q.; Ohta, S.; Audet, J.; Dvorak, H. F.; Chan, W. C. W., Analysis of nanoparticle delivery to tumours. *Nat. Rev. Mater.* 2016, 1 (5), 16014.

[9] Hume, D. A., The mononuclear phagocyte system. *Curr. Opin. Immunol.* 2006, 18 (1), 49-53.

[10] Bertrand, N.; Leroux, J.-C., The journey of a drug-carrier in the body: An anatomo-physiological perspective. *J. Control. Release.* 2012, 161 (2), 152-63.

[11] Zhang, Y. N.; Poon, W.; Tavares, A. J.; McGilvray, I. D.; Chan, W. C. W., Nanoparticle-liver interactions: Cellular uptake and hepatobiliary elimination. *J. Control. Release.* 2016, 240, 332-48.

[12] Kustanovich, A.; Schwartz, R.; Peretz, T.; Grinshpun, A., Life and death of circulating cell-free DNA. *Cancer Biol. Ther.* 2019, 20 (8), 1057-67.

[13] Ma, Y.; Brocchini, S.; Williams, G. R., Extracellular vesicle-embedded materials. *J. Control. Release.* 2023, 361, 280-96.

[14] Zelepukin, I. V.; Shevchenko, K. G.; Deyev, S. M., Rediscovery of mononuclear phagocyte system blockade for nanoparticle drug delivery. *Nat. Commun.* 2024, 15 (1), 4366.

[15] Van Rooijen, N.; Sanders, A., Kupffer cell depletion by liposome-delivered drugs: comparative activity of intracellular clodronate, propamidine, and ethylenediaminetetraacetic acid. *Hepatology* 1996, 23 (5), 1239-43.

[16] Diagaradjane, P.; Deorukhkar, A.; Gelovani, J. G.; Maru, D. M.; Krishnan, S., Gadolinium Chloride Augments Tumor-Specific Imaging of Targeted Quantum Dots. *Acs Nano* 2010, 4 (7), 4131-41.

[17] Wolfram, J.; Nizzero, S.; Liu, H. R.; Li, F.; Zhang, G. D.; Li, Z.; Shen, H. F.; Blanco, E.; Ferrari, M., A chloroquine-induced macrophage-preconditioning strategy for improved nanodelivery. *Sci. Rep.* 2017, 7, 13738.

[18] Belhadj, Z.; He, B.; Fu, J.; Zhang, H.; Wang, X.; Dai, W.; Zhang, Q., Regulating Interactions Between Targeted Nanocarriers and Mononuclear Phagocyte System via an Esomeprazole-Based Preconditioning Strategy. *Int. J. Nanomed.* 2020, 15, 6385-99.

[19] Ouyang, B.; Poon, W.; Zhang, Y. N.; Lin, Z. P.; Kingston, B. R.; Tavares, A. J.; Zhang, Y.; Chen, J.; Valic, M. S.; Syed, A. M.; MacMillan, P.; Couture-Senecal, J.; Zheng, G.; Chan, W. C. W., The dose threshold for nanoparticle tumour delivery. *Nat. Mater.* 2020, 19 (12), 1362-71.

[20] Nikitin, M. P.; Zelepukin, I. V.; Shipunova, V. O.; Sokolov, I. L.; Deyev, S. M.; Nikitin, P. I., Enhancement of the blood-circulation time and performance of nanomedicines via the forced clearance of erythrocytes. *Nat. Biomed. Eng.* 2020, 4 (7), 717-31.

[21] Mirkasymov, A. B.; Zelepukin, I. V.; Ivanov, I. N.; Belyaev, I. B.; Sh. Dzhalilova, D.; Trushina, D. B.; Yaremenko, A. V.; Yu. Ivanov, V.; Nikitin, M. P.; Nikitin, P. I.; Zvyagin, A. V.; Deyev, S. M., Macrophage blockade using nature-inspired ferrihydrite for enhanced nanoparticle delivery to tumor. *Int. J. Pharm.* 2022, 621, 121795.

[22] Liu, L.; Hitchens, T. K.; Ye, Q.; Wu, Y.; Barbe, B.; Prior, D. E.; Li, W. F.; Yeh, F. C.; Foley, L. M.; Bain, D. J.; Ho, C., Decreased reticuloendothelial system clearance and increased blood half-life and immune cell labeling for nano- and micron-sized superparamagnetic iron-oxide particles upon pre-treatment with Intralipid. Biochim. Biophys. *Acta (BBA)-General Subj.* 2013, 1830 (6), 3447-53.

[23] Liu, T.; Choi, H.; Zhou, R.; Chen, I. W., RES blockade: A strategy for boosting efficiency of nanoparticle drug. *Nano Today* 2015, 10 (1), 11-21.

[24] Martin-Alonso, C.; Tabrizi, S.; Xiong, K.; Blewett, T.; Sridhar, S.; Crnjac, A.; Patel, S.; An, Z.; Bekdemir, A.; Shea, D.; Wang, S. T.; Rodriguez-Aponte, S.; Naranjo, C. A.; Rhoades, J.; Kirkpatrick, J. D.; Fleming, H. E.; Amini, A. P.; Golub, T. R.; Love, J. C.; Bhatia, S. N.; Adalsteinsson, V. A., Priming agents transiently reduce the clearance of cell-free DNA to improve liquid biopsies. *Science* 2024, 383 (6680), eadf2341.

[25] Saunders, N. R. M.; Paolini, M. S.; Fenton, O. S.; Poul, L.; Devalliere, J.; Mpambani, F.; Darmon, A.; Bergere, M.; Jibault, O.; Germain, M.; Langer, R., A Nanoprimer To Improve the Systemic Delivery of siRNA and mRNA. *Nano Lett.* 2020, 20 (6), 4264-69.

[26] Augustine, R.; Hasan, A.; Primavera, R.; Wilson, R. J.; Thakor, A. S.; Kevadiya, B. D., Cellular uptake and retention of nanoparticles: Insights on particle properties and interaction with cellular components. *Mater. Today Commun.* 2020, 25, 101692.

[27] Bompard, J.; Rosso, A.; Brizuela, L.; Mebarek, S.; Blum, L. J.; Trunfio-Sfarghiu, A. M.; Lollo, G.; Granjon, T.; Girard-Egrot, A.; Maniti, O., Membrane Fluidity as a New Means to Selectively Target Cancer Cells with Fusogenic Lipid Carriers. *Langmuir* 2020, 36 (19), 5134-44.

[28] Yu, M.; Song, W.; Tian, F.; Dai, Z.; Zhu, Q.; Ahmad, E.; Guo, S.; Zhu, C.; Zhong, H.; Yuan, Y.; Zhang, T.; Yi, X.; Shi, X.; Gan, Y.; Gao, H., Temperature- and rigidity-mediated rapid transport of lipid nanovesicles in hydrogels. *Proc. Natl. Acad. Sci. U.S.A.* 2019, 116 (12), 5362-69.

[29] Li, Z.; Zhu, Y.; Zeng, H.; Wang, C.; Xu, C.; Wang, Q.; Wang, H.; Li, S.; Chen, J.; Xiao, C.; Yang, X.; Li, Z., Mechano-boosting nanomedicine antitumour efficacy by blocking the reticuloendothelial system with stiff nanogels. *Nat. Commun.* 2023, 14 (1), 1437.

[30] Han, J.; Collins, B. E.; Bengtson, P.; Paulson, J. C., Homomultimeric complexes of CD22 in B cells revealed by protein-glycan cross-linking. *Nat. Chem. Biol.* 2005, 1 (2), 93-7.

[31] Nsairat, H.; Khater, D.; Sayed, U.; Odeh, F.; Bawab, A. A.; Alshaer, W., Liposomes: structure, composition, types, and clinical applications. *Heliyon* 2022, 8 (5), e09394.

[32] Fukuda, A.; Tahara, K.; Hane, Y.; Matsui, T.; Sasaoka, S.; Hatahira, H.; Motooka, Y.; Hasegawa, S.; Naganuma, M.; Abe, J.; Nakao, S.; Takeuchi, H.; Nakamura, M., Comparison of the adverse event profiles of conventional and liposomal formulations of doxorubicin using the FDA adverse event reporting system. *PLOS ONE* 2017, 12 (9), e0185654.

[33] Suk, J. S.; Xu, Q.; Kim, N.; Hanes, J.; Ensign, L. M., PEGylation as a strategy for improving nanoparticle-based drug and gene delivery. *Adv. Drug Deliv. Rev.* 2016, 99, 28-51.

[34] Debets, M. F.; van Berkel, S. S.; Schoffelen, S.; Rutjes, F. P. J. T.; van Hest, J. C. M.; van Delft, F. L., Aza-dibenzocyclooctynes for fast and efficient enzyme PEGylation via copper-free (3+2) cycloaddition. *Chem. Commun.* 2010, 46 (1), 97-99.

[35] Besanceney-Webler, C.; Jiang, H.; Zheng, T.; Feng, L.; Soriano del Amo, D.; Wang, W.; Klivansky, L. M.; Marlow, F. L.; Liu, Y.; Wu, P., Increasing the Efficacy of Bioorthogonal Click Reactions for Bioconjugation: A Comparative Study. *Angew. Chem. Int. Ed.* 2011, 50 (35), 8051-56.

[36] Luo, D.; Carter, K. A.; Geng, J.; He, X.; Lovell, J. F., Short Drug–Light Intervals Improve Liposomal Chemophototherapy in Mice Bearing MIA PaCa-2 Xenografts. *Mol. Pharmaceutics* 2018, 15 (9), 3682-89.

[37] Allen, T. M.; Hansen, C.; Martin, F.; Redemann, C.; Yau-Young, A., Liposomes containing synthetic lipid derivatives of poly(ethylene glycol) show prolonged circulation half-lives in vivo. *BBA-Biomembranes* 1991, 1066 (1), 29-36.

[38] Lo, Y. M. D.; Zhang, J.; Leung, T. N.; Lau, T. K.; Chang, A. M. Z.; Hjelm, N. M., Rapid Clearance of Fetal DNA from Maternal Plasma. *Am. J. Hum. Genet.* 1999, 64 (1), 218-24.

[39] Diehl, F.; Schmidt, K.; Choti, M. A.; Romans, K.; Goodman, S.; Li, M.; Thornton, K.; Agrawal, N.; Sokoll, L.; Szabo, S. A.; Kinzler, K. W.; Vogelstein, B.; Diaz, L. A., Jr., Circulating mutant DNA to assess tumor dynamics. *Nat. Med.* 2008, 14 (9), 985-90.

[40] Matsumoto, A.; Takahashi, Y.; Chang, H. Y.; Wu, Y. W.; Yamamoto, A.; Ishihama, Y.; Takakura, Y., Blood concentrations of small extracellular vesicles are determined by a balance between abundant secretion and rapid clearance. *J. Extracell. Vesicles* 2020, 9 (1), 1696517.

[41] Morishita, M.; Takahashi, Y.; Nishikawa, M.; Sano, K.; Kato, K.; Yamashita, T.; Imai, T.; Saji, H.; Takakura, Y., Quantitative Analysis of Tissue Distribution of the B16BL6-Derived Exosomes Using a Streptavidin-Lactadherin Fusion Protein and Iodine-125-Labeled Biotin Derivative After Intravenous Injection in Mice. *J. Pharm. Sci.* 2015, 104 (2), 705-13.

[42] Luger, K.; Mäder, A. W.; Richmond, R. K.; Sargent, D. F.; Richmond, T. J., Crystal structure of the nucleosome core particle at 2.8 Å resolution. *Nature* 1997, 389 (6648), 251-60.

[43] Moghassemi, S.; Dadashzadeh, A.; Sousa, M. J.; Vlieghe, H.; Yang, J.; León-Félix, C. M.; Amorim, C. A., Extracellular vesicles in nanomedicine and regenerative medicine: A review over the last decade. *Bioact. Mater.* 2024, 36, 126-56.

Electronic Supplementary Material

Mononuclear phagocyte system blockade for enhanced liposome-assisted metabolic glycan labeling and circulating biomarker detection in mice

Pingping Feng[1,2], Tingbi Zhao[1,2], Rundong He[1,2], Lin Gan[1,2], Guangyu Hu[1,2], Xing Chen[1,2,3,4,5,6]✉, and Peng Dai[1,2,3,4]✉

[1]*College of Chemistry and Molecular Engineering, Peking University, Beijing 100871, China*
[2]*Beijing National Laboratory for Molecular Sciences, Peking University, Beijing 100871, China*
[3]*Synthetic and Functional Biomolecules Center, Peking University, Beijing 100871, China*
[4]*Key Laboratory of Bioorganic Chemistry and Molecular Engineering of Ministry of Education, Peking University, Beijing 100871, China*
[5]*Peking-Tsinghua Center for Life Sciences, Peking University, Beijing 100871, China*
[6]*College of Chemistry, Beijing Normal University, Beijing 100875, China*

✉ Address correspondence to Xing Chen ,xingchen@pku.edu.cn; Peng Dai, pengdai@pku.edu.cn

Table S1 The formulations and characteristics of 18 liposomal MPS blocker candidates and the liposomal Carrier

Liposomes	(DO+DS): Chol	DOPC	DSPC	Chol	Size (nm)	PDI
LP1		0	10	3	298.5±1.8	0.16±0.05
LP2		2	8	3	313.3±0.4	0.18±0.02
LP3	10:3	4	6	3	307.8±8.2	0.19±0.02
LP4		6	4	3	290.3±2.9	0.19±0.01
LP5		8	2	3	231.4±5.9	0.21±0.01
LP6		10	0	3	240.0±4.2	0.15±0.02
LP7		0	10	5	289.8±7.3	0.18±0.02
LP8		2	8	5	266.3±1.3	0.13±0.03
LP9	10:5	4	6	5	273.5±2.3	0.19±0.01
LP10		6	4	5	267.7±4.3	0.18±0.01
LP11		8	2	5	248.7±6.9	0.13±0.03
LP12		10	0	5	259.7±4.0	0.12±0.02
LP13		0	10	10	258.4±3.2	0.21±0.01
LP14		2	8	10	277.0±3.8	0.12±0.02
LP15	10:10	4	6	10	264.8±1.5	0.17±0.03
LP16		6	4	10	264.4±0.5	0.22±0.02
LP17		8	2	10	261.3±5.7	0.21±0.01
LP18		10	0	10	224.0±2.7	0.15±0.01
Carrier		DSPC: Chol: DSPE-PEG2000 = 56:39:5			183.1±1.4	0.01±0.01

Table S2 The encapsulated Cy5 concentrations for the LPs-Cy5

Liposomes	Cy5 (μM)
LP1-Cy5	98.1
LP2-Cy5	151.1
LP3-Cy5	113.7
LP4-Cy5	126.4
LP5-Cy5	159.8
LP6-Cy5	216.7
LP7-Cy5	81.6
LP8-Cy5	123.3
LP9-Cy5	116.5
LP10-Cy5	109.3
LP11-Cy5	130.8
LP12-Cy5	189.0
LP13-Cy5	81.1
LP14-Cy5	162.2
LP15-Cy5	80.3
LP16-Cy5	178.8
LP17-Cy5	145.7
LP18-Cy5	115.7

Table S3 The primer sequences.

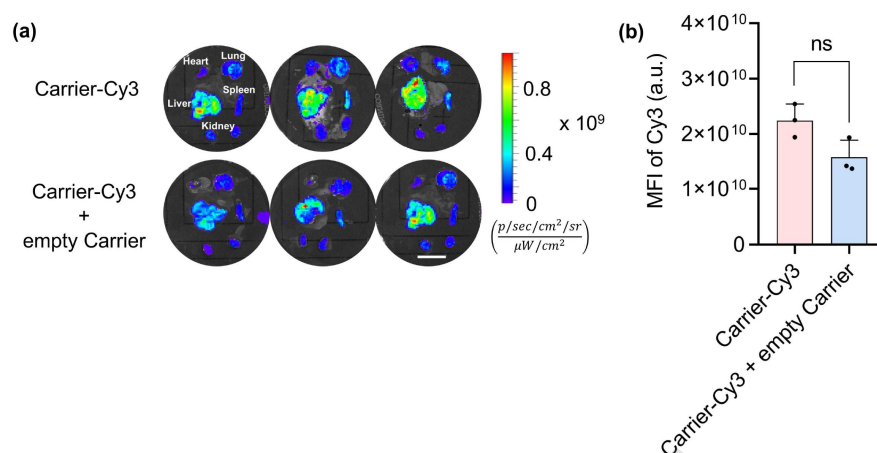| Primer	Sequence 5'–3'
Forward primers	CAGCCATTGCTCTTAGTCATCTC
Reverse primers	GGGAGACAGAAAAACATACACTGG

Figure S1 MPS blockade effect with empty liposomal Carrier. (a) Ex-vivo fluorescence imaging of various organs harvested from mice treated with the mixture of Carrier-Cy3 and empty Carrier at equal concentration for 0.5 h. Mice treated with Carrier-Cy3 alone served as the control. (b) Quantified fluorescence intensity of Cy3 in the liver. Data represent mean ± SEM from three biological replicates. *P* values were calculated by one-way ANOVA. a.u. arbitrary units. *ns* not significant.
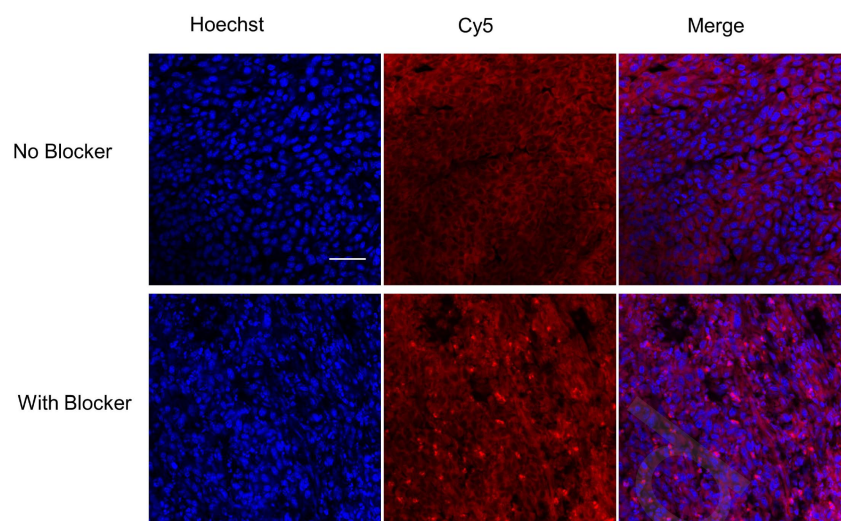
Figure S2 Confocal laser scanning microscopy (CLSM) images of frozen tumor sections from mice administered with the mixture of Blocker and Carrier, followed by injection of DBCO-Cy5. Scale bar, 45 μm.
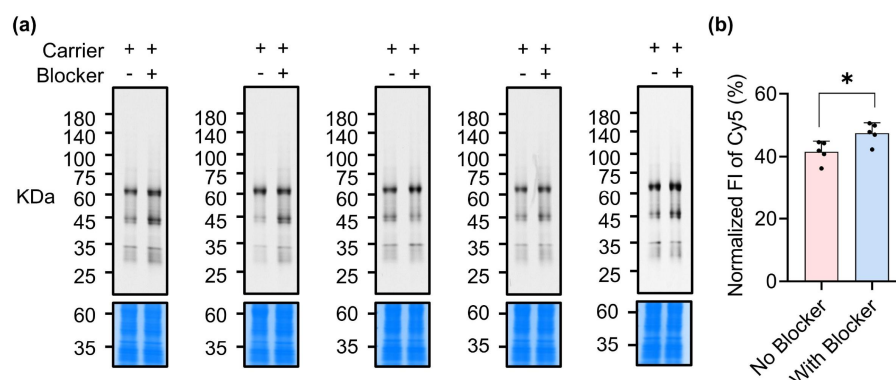
Figure S3 Quantitation of liposome-mediated incorporation of 9AzSia into tumor sialylated glycoproteins with or without Blocker. (a) In-gel fluorescence scanning of tumor lysates after reaction with alkyne-Cy5 for all five biological replicates. The Coomassie Brilliant Blue (CBB)-stained gel demonstrates comparable protein loading across samples. The first result was displayed in Figure 4f as a representative result. (b) Normalized fluorescence intensity of Cy5 in tumor lysates. FI, fluorescence intensity. Data represent mean ± SEM from five biological replicates. P values were calculated by one-way ANOVA. *$P < 0.05$.
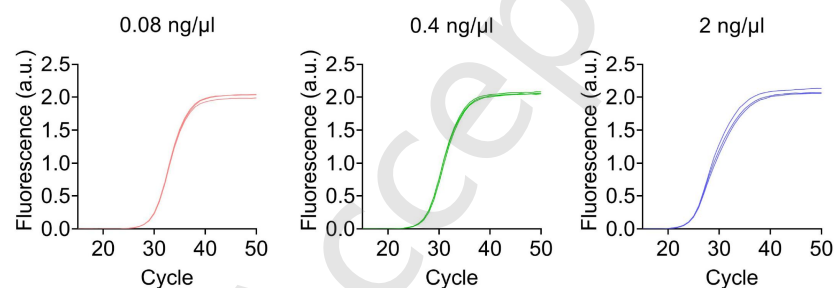

Figure S4 The qPCR amplification curves of genomic DNA (gDNA) at three different concentrations. FI, fluorescence intensity.
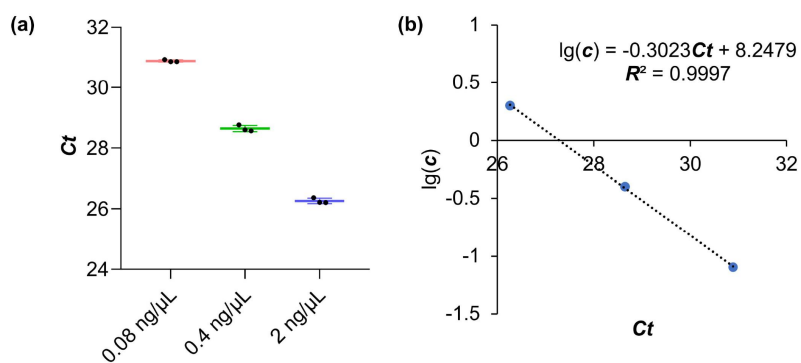
Figure S5 Standard curve for DNA concentration calculation. (a) Cycle threshold (*Ct*) values of gDNA at the concentrations of 0.08, 0.4, and 2 ng/μL. Data were from three biological replicates shown in Figure S4 in the ESM. (b) Standard curve connecting *Ct* values with the concentration of amplifiable DNA.